Journal Pre-proof

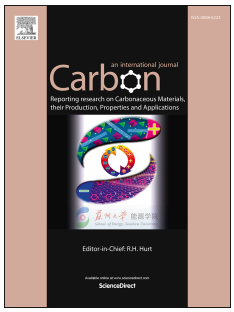

Freezing/melting of water in the confined nanospace of carbon materials: Effect of an external stimulus

Carlos Cuadrado-Collados, Ahmad A.A. Majid, Manuel Martínez-Escandell, Luke L. Daemen, Aleksandr Missyul, Carolyn Koh, Joaquin Silvestre Albero

PII: S0008-6223(19)31099-1

DOI: https://doi.org/10.1016/j.carbon.2019.10.081

Reference: CARBON 14743

To appear in: *Carbon*

Received Date: 23 September 2019

Revised Date: 28 October 2019

Accepted Date: 29 October 2019

Please cite this article as: C. Cuadrado-Collados, A.A.A. Majid, M. Martínez-Escandell, L.L. Daemen, A. Missyul, C. Koh, J. Silvestre Albero, Freezing/melting of water in the confined nanospace of carbon materials: Effect of an external stimulus, *Carbon* (2019), doi: https://doi.org/10.1016/j.carbon.2019.10.081.

GRAPHICAL ABSTRACT

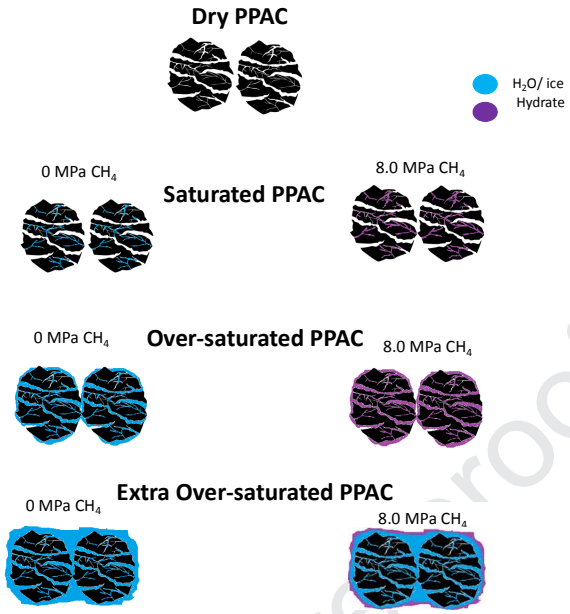

Freezing/melting of water in the confined nanospace of carbon materials: Effect of an external stimulus

Carlos Cuadrado-Collados,[1,2] Ahmad A.A. Majid,[2] Manuel Martínez-Escandell,[1] Luke L. Daemen,[3] Aleksandr Missyul,[4] Carolyn Koh,[2,*] and Joaquin Silvestre Albero[1,*]

[1]Laboratorio de Materiales Avanzados, Departamento de Química Inorgánica-IUMA, Universidad de Alicante, Spain.

[2]Chemical and Biological Engineering Department, Center for Hydrate Research, Colorado School of Mines, USA.

[3]Oak Ridge National Laboratory, Spallation Neutron Source, 1 Bethel Valley Road, Oak Ridge, USA.

[4] CELLS-ALBA Synchrotron, E-08290 Cerdanyola del Vallés, Spain.

Freezing/melting behavior of water confined in the nanopores of activated carbon materials has been evaluated using differential scanning calorimetry (DSC) at different water loadings, and after the application of an external stimulus. Under atmospheric pressure conditions, the DSC scans show a depression in the freezing/melting point of confined water compared to the bulk system. Interestingly, water confined in narrow micropores (pores below 0.7 nm) does not exhibit any phase transition, i.e. it is non-freezable water. Inelastic neutron scattering (INS) data confirm the presence of a distorted molecular assembly in narrow micropores, whereas synchrotron X-ray powder diffraction data (SXRPD) demonstrate the non-freezable nature of the water confined in these narrow-constrictions. Similar experiments under high-pressure CH_4 gives rise to a completely different scenario. Under high-pressure conditions methane hydrates are formed with a water-to-hydrate yield of 100% for the under-saturated and saturated samples, i.e. in the presence of an external stimulus even water in narrow micropores is prone to experience a liquid-to-solid phase transition. These results confirm the beneficial role of carbon as a host structure to promote nucleation and growth of methane hydrates with faster kinetics and a higher yield compared to the bulk system and to other porous materials.

[*] Corresponding authors:

Carolyn Koh; Email: ckoh@mines.edu
Joaquin Silvestre-Albero; Email: joaquin.silvestre@ua.es

1. Introduction

The freezing/melting of water in the confined environment of nanoporous materials is a very important phenomenon to understand daily life processes such as the deterioration of outdoor buildings under extreme temperature conditions, the performance of liquid-phase batteries upon a drastic temperature alteration, or in the formation of natural hydrates in seawater sediments. It is widely accepted in the literature that the strong adsorption potential in narrow cavities and the presence of steric restrictions give rise to important changes in the molecular assembly structure, and an associated decrease in the water activity compared to bulk water [1]. These alterations are reflected in anomalous phenomena, for instance in the freezing/melting performance. A simple capillary theory such as the Gibbs-Thomson equation is able to predict a shift in the freezing temperature as a function of the pore width (Equation 1).

$$\frac{\Delta T_f}{T_{fb}} = -2\,\frac{(\gamma_{ws}-\gamma_{wl})v}{H\lambda_{fb}} \qquad (1)$$

where T_{fb} is the bulk freezing temperature, γ_{ws} and γ_{wl} are the corresponding wall-solid and wall-fluid surface tensions, v is the molar volume of the liquid, $\lambda_{fb}$is the latent heat of melting in the bulk and *H* is the pore width. This classical thermodynamic equation anticipates a shift in the freezing temperature for a given liquid that depends on the nature of the porous solid, through the wall-solid and wall-fluid interactions. Traditionally a decrease in the freezing temperature has been observed for water confined in porous silicas and silica-based materials [2,3]. Following the Gibbs-Thomson equation, Morishige et al. reported a perfectly linear relationship between the melting point depression and the capillary condensation for nitrogen at 77 K, and indirectly, with the pore size width [3]. However, this behavior is not straightforward in the case of other porous solids, e.g. carbon materials. Grand canonical Monte Carlo simulations for methane adsorbed in different porous materials (from graphitic carbon to hard walls) with slit-shaped morphology anticipated a different scenario [4]. Theoretical predictions anticipate that the fluid-wall interactions determine the direction and magnitude of the shift in the freezing temperature. In other words, an increase in the freezing temperature relative to that of the bulk is predicted for strongly attractive walls (e.g., graphitic carbon), whereas the opposite takes place for hard walls with very low

fluid-wall interactions. Indeed, Watanabe et al. observed an increase in the melting temperature (~ 16-20 K) for benzene confined in graphitic micropores, in close agreement with GCMC [5]. Taking into account the hydrogen bonding ability of water, *a priori*, it is easy to anticipate a different performance for water confined in the porous structure of carbon materials, compared to methane or benzene.

Despite the importance of water adsorption in carbon materials, the number of studies dealing with the evaluation of these freezing/melting processes is rather scarce. Iiyama et al. observed that under confined conditions water exhibits a much ordered structure compared to bulk liquid water but with a smaller number of nearest-neighbor molecules [6,7]. In-situ small-angle X-ray scattering (SAXS) studies and Reverse Monte Carlo simulations confirm the water adsorption mechanism in a hydrophobic environment (e.g., carbon cavities) through cluster-like assemblies [8,9]. The water adsorption mechanism in carbon materials can be explained due to the low water-carbon interactions and the strong intermolecular interactions (20 kJ/mol) that promote clustering [7]. Neutron scattering experiments of water confined in carbon nanotubes also reported a novel and unique dynamic behavior of water under sub-nanometer axial confinement, related to the appearance of water molecules with a coordination number of about two [10,11]. Despite these anomalous evidences, there are no studies in the literature dealing with the evaluation on how these fluid-wall interactions can affect/modify the freezing/melting performance of water under confined conditions. A similar situation happens upon an external stimulus. Despite the importance of the freezing/melting behavior of water-methane mixtures under a confined carbon environment and the associated methane hydrate formation/dissociation, the number of studies reported in the literature using DSC is rather scarce. The understanding of these crystal nucleation processes in carbon materials are extremely important taking into account that activated carbon constitutes the most promising material to date to store high-pressure methane in the form of hydrate, as compared to other materials such as zeolites or MOFs [12-18]. These confined hydrates prepared artificially are considered a potential solution to store and transport natural gas, i.e. the so-called solidified natural gas.

With this in mind, the main goal of this manuscript is the evaluation of the freezing/melting performance of water adsorbed in a high-surface area activated carbon under different water-supplying conditions. These experiments will be performed under atmospheric pressure conditions, to evaluate the liquid water-to-ice

formation/dissociation in confined nanospaces, and under high-pressure methane, to evaluate the liquid water-to-methane hydrate formation/dissociation.

2. Experimental section

A high-surface area activated carbon (PPAC) was prepared using petroleum pitch as the carbon precursor through a chemical activation route. A detailed description of the synthesis process can be found in our earlier work [19]. Briefly, the synthesis involves the activation of the pyrolyzed petroleum pitch with potassium hydroxide (KOH) (KOH: carbon precursor ratio of 6:1) at 1073 K for 2h under a nitrogen flow (50 ml/min), followed by a washing step using HCl and H_2O until complete removal of the chemical agent (neutral pH).

The loading of the activated carbon with water was carried out using a humidifier under a 100% relative humidity. The amount of water pre-adsorbed is denoted as R_w, i.e. mass of water per mass of dry carbon. The preparation of the saturated sample was performed by placing the activated carbon inside the humidifier and following the water uptake (weight increase) daily until constant weight. Under-saturated samples were prepared in a similar way but collecting the samples at different time intervals (before saturation). Finally, oversaturated samples were prepared through the incorporation of additional water to the fully saturated carbon using a calibrated micropipette until the desired R_w.

Textural properties of the synthesized samples were evaluated by gas physisorption: i) nitrogen adsorption at 77.4 K and ii) carbon dioxide adsorption at 273 K. Gas adsorption measurements were performed in a home-made fully automated manometric apparatus designed and constructed by the Advanced Materials Group (LMA) and now commercialized by Gas to Materials (www.g2mtech.com). Before the adsorption measurements, the samples were subjected to an outgassing step for 4 h at 523 K under ultra-high vacuum (10^{-3} Pa). Nitrogen adsorption data were used to determine: (i) the total pore volume (V_t) at a relative pressure of 0.95, (ii) the BET-specific surface area (S_{BET}) and (iii) the micropore volume (V_{N2}) using the Dubinin–Radushkevich (DR) equation. The difference between V_t and V_{N2} is considered to be the mesopores volume (V_{meso}). CO_2 adsorption data at 273 K were used to determine the narrow micropore volume (V_{CO2}) after application of the DR equation.

Two different differential scanning calorimeters (DSC) were used in this study:

1.-DSC measurements without any external stimulus were performed in a DSC Q100 apparatus (TA Instruments) using hermetically sealed aluminum pans. A typical experiment consists of a cooling-heating cycle under 50 ml/min N_2. The sample is first cooled from 293 K down to 183 K at a cooling rate of 1 K/min. Once at the lower temperature, an isothermal step is performed for 5 min, followed by a heating step (rate of 1 K/min) back to 293 K.

2.-For the DSC measurements under high pressure, measurements were conducted using a micro-differential scanning calorimeter (μ-DSC, Setaram Inc.) equipped with high pressure cells. The high pressure cells can withstand up to 15.4 MPa. The HP-DSC has an operating temperature range from 393 K down to 228 K. In this work, measurements were conducted by placing ≅ 30 mg of activated carbon loaded to the desired water ratio (R_w) inside the DSC furnace. The cell containing the sample was tightly sealed and placed in the equipment. In order to avoid the effect of air on the experimental results, the cell was purged with the experimental gas composition for a minimum of 3 times. Next, the cell was pressurized with methane gas (99.997% purity, General Air) to 12.5 MPa. The cell was left for a few minutes (up to 3 minutes) to ensure that there was no gas leak. A gas leak can affect the overall results of the heat traces. After this step, the sample underwent heating and cooling cycles for hydrate formation/dissociation. In each cycle, the sample was heated from room temperature conditions to 303 K at a rate of 0.5 K/min. The sample was left under these conditions for 3 hours to achieve equilibrium. Next, the sample was cooled from 303 K to 233 K at rate of 0.15 K/min for hydrate formation. Following this step, the sample was heated back to 303 K at rate of 0.15 K/min to observe the hydrate dissociation peak. This heating and cooling steps were repeated for another 2 cycles.

Synchrotron X-ray powder diffraction data (SXRPD) were collected on the powder diffraction endstation of the MSPD beamline at synchrotron ALBA in Spain, using a MYTHEN detector and a wavelength of 0.4227 Å. The experiments were performed in an *ad hoc* capillary reaction cell (fused silica capillary, inner diameter 0.7 mm, outer diameter 0.85 mm). Before the experiment the water pre-adsorbed carbon samples were placed inside the cell, which was connected via a capillary line to a gas-handling and a

vacuum line. An Oxford Cryostream 700 was used to control the temperature of the sample.

Inelastic neutron scattering (INS) measurements were performed at the VISION beamline (BL-16B) of the Spallation Neutron Source (SNS), Oak Ridge National Laboratory (ORNL), USA. About 200 mg of the D_2O pre-adsorbed activated carbon was loaded in an Al sample holder connected to a gas handling system. The blank sample was first evacuated for 2h at 253 K and subsequently cooled down to 5 K. Once at this temperature, the INS spectrum was collected for several hours (the background for the instrument and sample holder is negligible in this case since the hydrogenous sample scatters neutrons very strongly). After the background measurement, the carbon sample was loaded with CH_4 at 275 K up to 8.0 MPa. The dosed sample was cooled down to 5 K and the INS was re-measured for several hours.

3. Results and discussion

3.1. Textural characteristics of the activated carbon

The high-surface area activated carbon (PPAC) was prepared from a petroleum residue (VR) using KOH as a chemical activating agent. A detailed description of the synthesis conditions can be found elsewhere [12,19]. Briefly, the synthesized activated carbon has a widely developed porous structure combining a high proportion of micro- and mesopores (Figure S1). The BET apparent surface area is around 3700 m^2/g with a micropore volume, V_{N2}, of 1.20 cm^3g^{-1} and a narrow micropore volume, V_{CO2}, of 0.60 cm^3g^{-1} (Figure S2) (see Table S1 for a summary of the textural properties). The selection of the PPAC activated carbon is based on the excellent performance exhibited by this material as a host structure to promote the nucleation and growth of confined methane-hydrate nanocrystals [12,19]. Under proper experimental conditions, this material is able to store more than 60 wt.% CH_4 in the form of gas hydrate. To our knowledge, this is the best result described in the literature so far for high-pressure methane storage.

3.2. Water adsorption isotherms at 298 K in sample PPAC

Figure S3 shows the water adsorption/desorption isotherms for sample PPAC up to 0.88 and 0.94 relative pressure. As expected, the water adsorption isotherms exhibit a type III behavior characteristic of porous networks with a small fluid-surface affinity (XPS analysis of sample PPAC reports an atomic composition of 97.3% carbon and 2.7 % oxygen). Despite the high hydrophobicity of sample PPAC, water isotherms exhibit a sudden increase in the amount adsorbed above $p/p_0 > 0.7$, attributed to the filling of the micropores and small mesopores. The total amount adsorbed at 0.88 relative pressure is 0.2 g/g, while at 0.94 this value goes up to ≅ 1 g/g. At this point it is important to highlight that at saturation (in the presence of 100% humidity) the amount adsorbed reaches a value as high as 2.4 g/g (or cm^3/g), in close agreement with the total pore volume obtained from the N_2 adsorption isotherms. This agreement reflects that water at saturation (R_w = 2.4) must be filling narrow/wide micropores and small mesopores in PPAC.

3.3. Confined water in the absence of an external stimulus

3.3.1. Differential scanning calorimetry (DSC) analysis of confined water

The freezing - melting performance of water confined in the cavities of the PPAC sample has been evaluated after loading with different water ratios, R_w (gram H_2O per gram of carbon). Table 1 reports the different water ratios evaluated, from under-saturation (R_w < 2.1), to saturation (R_w = 2.4) and oversaturation conditions (R_w = 4.1).

Table 1. Description of the different water ratios, R_w, evaluated.

	Under-saturated												Saturated	Over-saturated
sample number	1	2	3	4	5	6	7	8	9	10	11	12	13	14
R_w (g_{H2O}/g_{PPAC})	0.02	0.03	0.08	0.15	0.22	0.46	0.64	0.85	0.95	1.2	1.7	2.1	2.4	4.1

The main goal is to perform a progressive filling of the porous network, from narrow to wide micropores and small mesopores in order to get further insight into the freezing/melting processes in each of these cavities. It is widely accepted in the literature that freezing proceeds via homogeneous nucleation under non-equilibrium conditions with a large supercooling, independent of the pore size, whereas the melting process is well-described by the Gibbs-Thomson equation [20]. Figure 1 shows the

different DSC profiles obtained during cooling and warming in the temperature range 183 K to 293 K, for the different samples evaluated. The freezing and melting temperature for the bulk water, using the same equipment (see Figure S4), is included as a reference. Bulk water exhibits a sharp freezing peak at 255 K, whereas melting takes place at 275 K (onset at 273 K), in close agreement with thermodynamics.

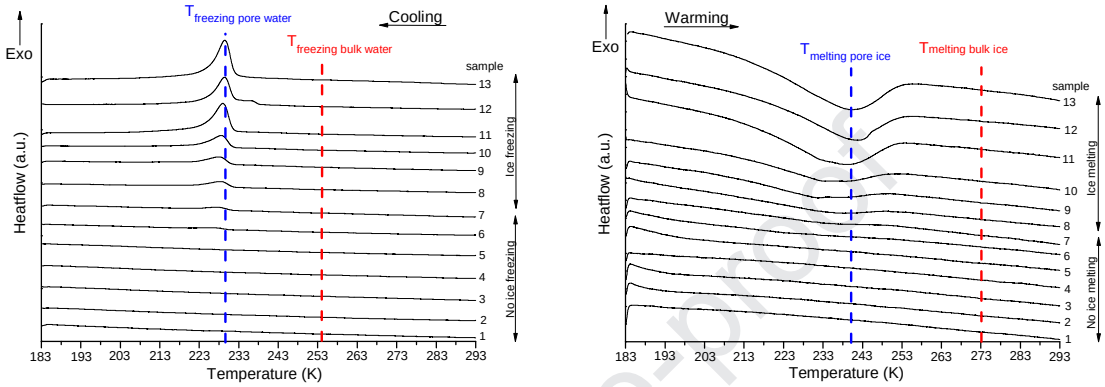

Figure 1. DSC profiles for cooling and warming of H_2O confined in the nanoporous structure of activated carbon materials up to saturation.

The DSC profiles for the water-loaded PPAC samples exhibit two well-defined regions. Below a certain R_w ratio (sample 1 up to 7; $R_w < 0.6$) the DSC profile is completely flat both for cooling scan, down to 183 K, and the melting scan, back to 293 K. This result constitutes clear evidence on the anomalous performance of water confined in nanoporous activated carbons. Even under large sub-cooling conditions (183 K), confined water is not able to experience the traditional freezing/melting processes. Interestingly, the R_w ratio for this unusual performance corresponds to the narrow micropore volume (V_{CO2}) deduced from the CO_2 adsorption data at 273 K, i.e. 0.6 cm^3/g or 0.6 g/g. Apparently, water confined in narrow micropores under high confinement conditions is not able to experience a liquid-to-solid transition, i.e. it is non-freezable water. The presence of atypical dynamic features for confined water in carbon nanotubes has been widely described in the literature using neutron scattering techniques [10,11]. The presence of a novel and unique dynamic behavior is related to the appearance of water molecules characterized by a coordination number of about two, promoted by the sub-nanometer axial confinement. Furthermore, this observation is in close agreement with theoretical predictions using grand canonical Monte Carlo for

another probe molecule, methane [4]. GCMC simulations predict the absence of freezing transitions for pore widths below 5.3 σ on graphitic systems, i.e. pores with only 4 adsorbed layers of methane.

Above the critical R_w ratio, cooling scans start to develop an exothermic peak at around 229 K that grows progressively with the amount of water pre-adsorbed up to a maximum in the saturated sample (sample number 13). Compared to bulk water, the freezing of water confined in the cavities of the activated carbon takes place at a much lower temperatures (229 K vs. 255 K). Importantly, the freezing temperature for the confined water is independent of the amount pre-adsorbed, i.e. independent of the kind of cavity filled with water (either wide micropores or small mesopores). A similar insensitivity to the pore width was described for benzene melting in carbon materials but in the microporous range (pore range 0.75-1.2 nm) [5]. The kinetic super-cooling required in under-saturation conditions perfectly fits with the Gibbs-Thomson equation described above. Based on these observations, one can speculate that water confined in narrow micropores is non-freezable, whereas excess water above this critical R_w (located preferentially in wide micropores and small mesopores) exhibits a rather similar kinetic super-cooling effect. Taking into account the hydrophobic nature of the carbon surface, the presence of rather small fluid-wall interactions will justify the observed shift to lower temperatures, in accordance with GCMC [4]. A shift to lower temperatures was also described by Sliwinska-Bartkowiak at al. for water confined in activated carbon fibers [21]. However, at this point it is important to highlight that in systems with a higher hydrophilicity (e.g. silicas) and larger fluid-wall interactions, the observed shift in the water freezing is also negative, thus anticipating the complexity of the freezing/melting process [2]. Additional parameters such as the pore geometry and polarity of the probe molecule may account for these discrepancies [21,22].

Concerning the melting behavior, a single, broad DSC peak can be observed at 240 K for sample 8 and above. Compared to melting of bulk water (273 K), the melting of confined water is promoted at lower temperatures, in close agreement with the Gibbs-Thomson equation. Last but not least, the difference between the freezing and the melting temperature for confined water (≅ 11 K) clearly anticipates the presence of an important hysteresis loop, similar to that described before for silicas [2]. This hysteresis is associated with the nature of both processes: while melting is generally a one-step process, freezing involves first a nucleation and then a crystal growth around the initial cluster or nucleus [2]. In addition, freezing is a stochastic process that is controlled

kinetically, which means that depending on the conditions of the experiment like amount and arrangement of the water, cooling ramp, etc., nucleation may happen at different temperature points. On the contrary, melting is an equilibrium process controlled thermodynamically that provides real information about the phase transition. For these reasons, the melting process is generally used to quantify temperature and enthalpy values for the phase change.

The situation is more complex for the oversaturated sample (R_w = 4.1), i.e. when water is pre-adsorbed in micropores, mesopores and larger cavities. As it can be observed in Fig S4, oversaturation gives rise to a completely different scenario. Excess water in PPAC (located preferentially in large macropores and external surface) freezes at a higher temperature compared to bulk water (266 K vs. 255 K), whereas confined water preserves the contribution at 229 K. In other words, while the surface of the activated carbon acts as a nucleation platform promoting the solid-ice phase formation, under confinement conditions the reverse effect takes place, with a partial inhibition of the freezing process. A similar situation takes place during warming, with the confined water melting taking place at 240 K and the external surface melting taking place at 273 K.

To further explore the behavior of confined water towards freezing/melting, the associated melting enthalpy ($-\Delta H_m$) has been evaluated for the different water-loaded samples. The enthalpy values have been compared using in the calculations the total amount of water pre-adsorbed (kJ/mol) and after normalization using the total amount of "freezable" water, i.e. the water present in wide micropores and mesopores, excluding the water in narrow micropores.

Table 2. Enthalpy of melting calculated from the DSC experiments and onset temperature for the melting process.

Sample	R_w, g_{H2O}/g_{PPAC}	T_m, K	$-\Delta H_m$, kJ/mol	$-\Delta H^*_m$, kJ/mol
8	0.85	240.15	0.72	2.36
9	0.95	240.25	0.73	2.36
10	1.22	240.15	0.77	2.29
11	1.71	240.25	0.71	2.39

12	2.15	241.25	0.74	2.36
13	2.4	241.25	0.76	2.32
bulk water	-	273.15	5.99	-

* Normalized excluding the amount of water in narrow micropores

As it can be appreciated in Table 2, the melting of ice confined in wide micropores and small mesopores is quite independent of the water loading ratio (and indirectly of the pore size) with a single peak located at around 240-241 K. Interestingly, the melting enthalpy is rather constant for the different loading ratios, with an average value close to -0.72 kJ/mol. This result suggests that once the critical R_w is reached, any additional water added to the porous network is prone to freeze with a similar enthalpy value. Since this $-\Delta H_m$ is far below the value obtained for bulk water (-5.99 kJ/mol), the enthalpy values were recalculated considering only the water pre-adsorbed in wide micropores and mesopores, i.e. the water susceptible to freeze. Even under this assumption, enthalpy values do not exceed -2.36 kJ/mol, i.e. even though pre-adsorbed water can freeze and melt, the enthalpy of this process is far from the bulk process (61% lower). The insensitivity of the melting enthalpy to the pore width and its smaller value compared to the bulk is in close agreement with previous measurements for benzene confined in microporous carbons [5]. The presence of an anomalous molecular assembly with a lower number of near-neighbor water molecules, and a smaller number of hydrogen bonds, can justify the much lower enthalpy obtained. However, at this point it is important to highlight that a similar enthalpy value (-2.43 kJ/g) was obtained by our research group for purely mesoporous carbon materials in the pore size range 5-20 nm with less confinement constrains (data not shown). Similar studies described in the literature by Handa et al. for porous Vycor glass have reported also a reduction in the melting heat of water, although to a lesser extend (16-48% smaller for Vycor glass vs. 89% smaller in this work) [2]. In the specific case of silicas the lower enthalpy was attributed to the presence of bound, non-freezable, water even in large micropores and mesopores (around two-three monolayers of bound water) [23,24]. This assumption cannot be ruled out to justify the results obtained for carbon materials, although the presence of bound water seems less probable in hydrophobic environments.

3.3.2. Inelastic neutron scattering of confined water

One of the most powerful techniques to evaluate the performance of water in confined nanospaces is inelastic neutron scattering (INS). INS allows evaluating the librational and vibrational modes of water molecules at cryogenic temperatures (5 K) in confined environments. Due to the restricted space of water in narrow cavities, a significant inhibition of the intermolecular motions is expected [10,11]. The INS spectra reported in Figure 2 is dominated by the vibrational (0-40 meV) and librational modes (40-110 meV) at low energy transfer, while high-frequency O-H bending modes can be observed above 110 meV. The INS spectra have been measured at 5 K using two different D_2O pre-loadings to evaluate the performance of deuterated water confined in narrow micropores (low loading; R_w = 0.6) and wide micropores + small mesopores (high loading; R_w =2.4).

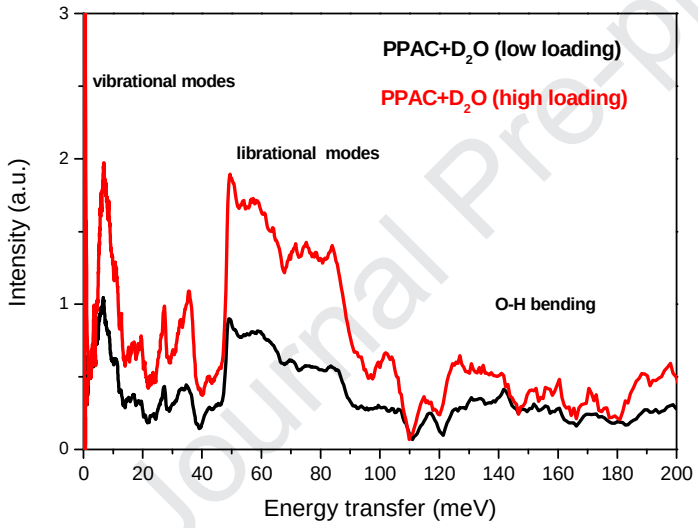

Figure 2. Inelastic neutron scattering spectra of D_2O confined in the porous structure of PPAC sample at low loading (R_w = 0.6) and high loading (R_w = 2.4). Experiments are performed at 5 K.

Figure 2 clearly shows that the D_2O dynamics do not exhibit important changes in terms of energy transfer between the two types of confined water, i.e. no shifts could be seen. However, a general suppression of the structural dynamics can be found over the whole energy transfer range evaluated, this effect being more drastic in the specific case of the H-O-H bending modes. The suppression of the H-O-H bending modes, preferentially in the low energy tail is in close agreement with the results described by Kolesnikov et al.

[20] for water confined in nanotubes. These results confirm that below the critical R_w of 0.6, deuterated water is present in the narrow cavities of the activated carbon although with different rotational, librational and bending dynamics compared to D_2O in wider micropores and mesopores.

3.3.3. Synchrotron X-ray powder diffraction (SXRPD) evaluation of confined water

To further evaluate the nature of confined water and the liquid water-to-ice conversion, sample PPAC pre-adsorbed with different water loadings (R_w<0.6 and R_w=2.4) has been submitted to a cooling scan down to 173 K using in-situ synchrotron X-ray powder diffraction. The main goal of this experiment was to ascertain the temperature range for the liquid water-to-ice formation and the nature of the ice crystals formed under confined conditions. Previous studies described in the literature for silica and carbon/silica materials did not provide a clear answer about the crystallographic structure of the confined ice nanocrystals, either cubic ice (I_c) or hexagonal ice crystals with a high proportion of defect sites [3]. Figure 3 shows the SXRPD profiles for the PPAC at low and high water loading at temperatures ranging from 298 K down to 173 K. At this point it is important to highlight that the reported temperatures corresponds to those measured at the cryocooler end located 0.8 cm from the PPAC capillary, i.e. a certain shift between the measured temperature and the real temperature is expected in our experimental setup.

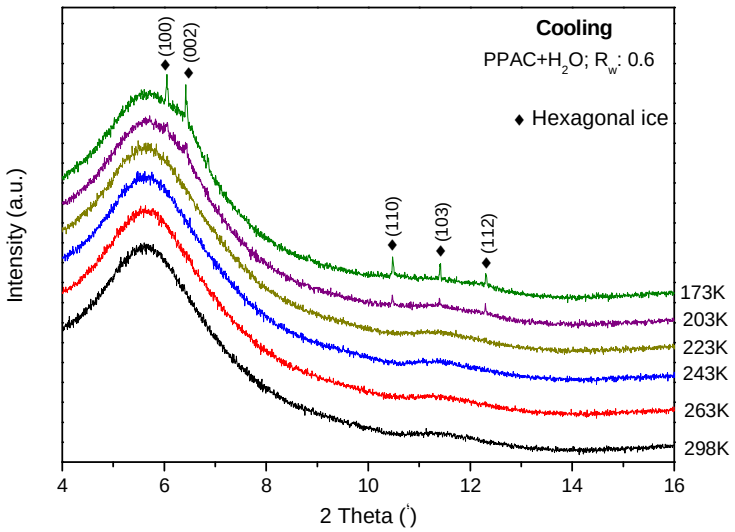

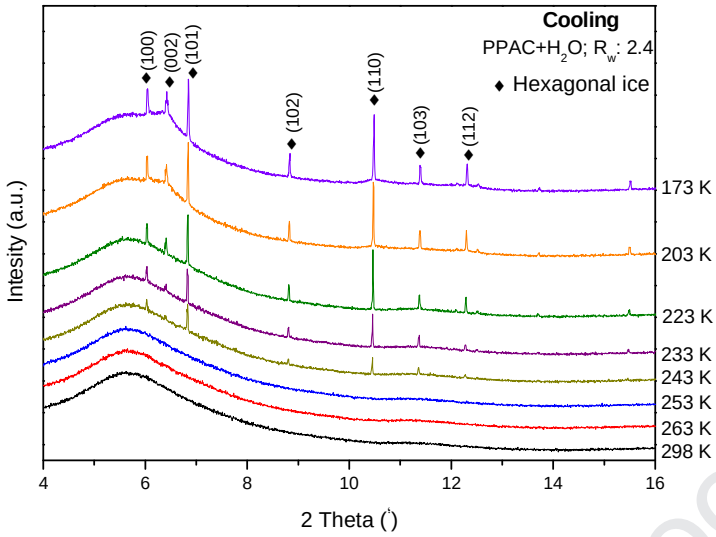

Figure 3. Synchrotron XRPD profiles for the PPAC activated carbon pre-adsorbed with a low (upper panel) and high (lower panel) water content.

As expected, the XRPD pattern of the sample containing water in narrow micropores (under-saturated sample; $R_w = 0.6$), does not exhibit any liquid-to-ice transition over the whole temperature range evaluated. Only at relatively low temperatures (200 K and below), small peaks can be seen. These peaks can be unambiguously assigned to hexagonal ice (I_h) with a certain distortion, the main contributions appearing at 6.2º, 6.8º, 7.0º and 10.5º, corresponding to (100), (002), (101) and (110), respectively. This result is very interesting because even though we cannot observe any change in enthalpy during the DSC scan down to 183 K, SXRPD results show that some water can be converted to ice but only at relatively low temperatures and to a very small extend (very low yield).

An increase in the amount of water incorporated up to saturation gives rise to well-defined hexagonal ice peaks already at "high" temperatures (ca. 243 K), in close agreement with the DSC analysis reported in Figure S4 for oversaturated PPAC (taking into account the temperature shift due to the different experimental setup). Last but not least, it is important to highlight the presence of hexagonal ice (I_h) in the confined nanospace of carbon at temperatures as low as 172 K. Previous studies in the literature using porous silica and hydrogels have reported the presence of exclusively cubic ice (I_c) at these temperature conditions [25,26].

3.4. Confined water in the presence of an external stimulus

3.4.1. Differential scanning calorimetry (DSC) analysis of confined water under high-pressure methane

The freezing/melting performance of water pre-adsorbed PPAC samples has been evaluated in the presence of an external stimulus, i.e. in the presence of high-pressure methane. Under these conditions the behavior of confined water must be altered/modified due to the possibility to nucleate small nanocrystals of methane hydrate. These experiments have been performed using another DSC equipment (see experimental section for further details) able to work at high pressure, although with a limited temperature range (down to 233 K). For the sake of clarity, the experiments have been restricted to three samples, i.e. saturated PPAC (sample 13; R_w = 2.4), and oversaturated samples (sample 14; R_w = 4.1, and a new sample incorporated, sample 15; R_w = 11). Figure 4 shows the DSC profiles for the three selected samples after pre-adsorption with water (upper panel), similar samples in the presence of 3.5 MPa CH_4 (middle panel) and in the presence of 8.0 MPa CH_4 (lower panel). Bulk water is included for the sake of comparison. The first set of experiments (in the absence of high pressure methane-upper panel) was performed in order to have a direct comparison between the two DSC equipments used in this study. This comparison is important since the high-pressure system has lower sensitivity and requires a larger amount of sample with the corresponding changes in the freezing/melting performance. These differences are clearly reflected in Figure 4, upper panel. As expected, the saturated sample (R_w = 2.4) exhibits a perfectly flat profile during cooling and warming, in close agreement with experimental results described above for the other DSC. Water confined in micropores and small mesopores can only freeze at 231 K or below, outside the temperature range of the actual DSC equipment. Samples oversaturated (samples 14 & 15) exhibit some sharp DSC peaks in the temperature range 268 K - 253 K due to the freezing of water located in large cavities (macropores and external surface), the freezing of this water being promoted compared to the behavior in bulk water. The promotion of the freezing process in the presence of activated carbon is in close agreement with the results described above using the other equipment. Furthermore, the presence of 2-3 peaks during the cooling process must be attributed to the larger amount of water (larger droplets) used in the actual experiments. Interestingly, all these

differences vanish in the warming step with a single melting peak located at 273-274 K, independently of the pre-adsorption ratio and the confinement effects.

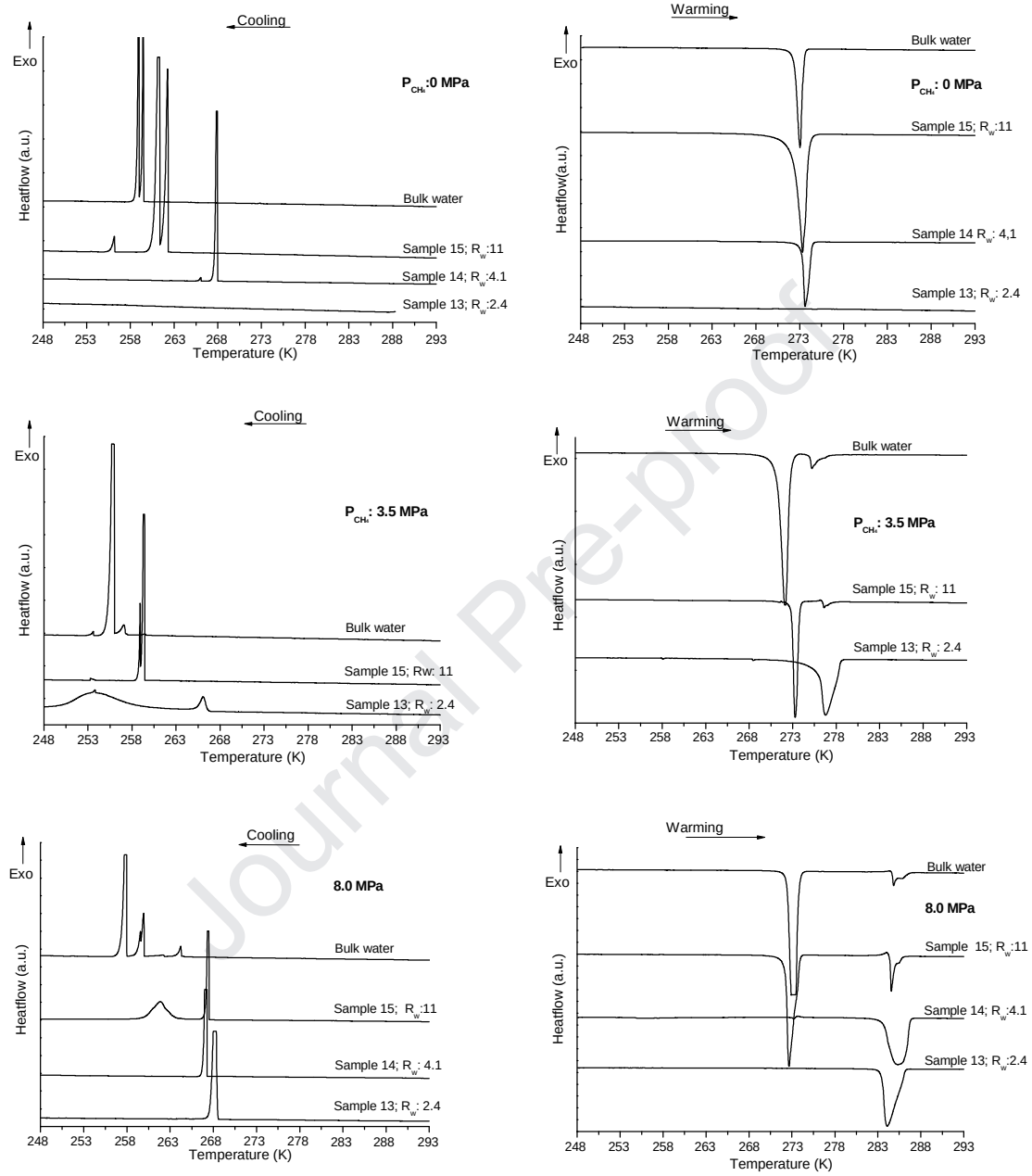

Figure 4. DSC profiles, cooling (left column) and warming (right column), for sample PPAC at different pre-adsorption ratios (R_w) and under different methane pressure conditions, i.e. 0 MPa (under atmospheric pressure conditions), 3.5 MPa and 8.0 MPa.

Interestingly, the scenario changes drastically after the incorporation of methane at high-pressure. At 3.5 MPa the saturated sample (sample 13) changes from a flat profile

(in the absence of an external stimulus) to the development of two freezing peaks, a sharp contribution at 266 K and a broad contribution at 254 K. An increase in the pressure to 8.0 MPa produces the complete disappearance of the 254 K contribution, and the growing of a single sharp peak at 268 K. A similar sharp contribution can be observed at 8.0 MPa for samples 14 and 15 at around 265 K. In addition, sample 15 with a large excess of water exhibits a broad contribution at 262 K. A comparison of the DSC profiles before and after incorporation of high-pressure methane suggest that the contributions at 265-268 K must be associated with the methane hydrate formation (these contributions are favored at high pressure), whereas the broad contributions at lower temperatures must be associated with confined water. At this point it is interesting to highlight that the saturated sample (sample 13) develops this confined water freezing peak only in the presence of 3.5 MPa, while it does not at atmospheric pressure (a flat DSC profile was obtained). Either the incorporation of methane promotes the freezing of the water confined in micropores and mesopores (including narrow micropores) at a higher temperature or the incorporation of high pressure methane promotes the mobility of water confined in narrow cavities to larger cavities (where it may be susceptible to freeze).

All these changes taking place in the presence of high-pressure methane can be more clearly appreciated in the melting profiles. Whereas in the absence of an external stimulus water exhibits a single DSC contribution at around 273 K, due to the melting of ice in large cavities and external surface (only samples above saturation show this contribution), the scenario changes under high-pressure conditions. At 8.0 MPa, saturated sample (R_w = 2.4) exhibits a single sharp melting peak at 285 K (onset at 283 K). This contribution could be attributed to the melting of the methane hydrate in confined cavities. The presence of a simple contribution is preserved in the sample with micropores and mesopores filled with water (R_w = 4.1). Only samples with a large excess of water (R_w = 11) exhibit a second contribution at 273 K due to melting of ice water, in close agreement with the results in the bulk phase.

These results confirm that i) confined water exhibits a different freezing/melting performance under high-pressure methane conditions, ii) samples with a water ratio $R_w \leq 4.1$ exhibit a single hydrate peak, thus anticipating a complete water-to-hydrate conversion (no ice can be appreciated), iii) freezing and melting of confined methane hydrate is shifted to higher temperatures (+12 K for melting) compared to confined ice, iv) stability of confined hydrates is rather similar to bulk hydrates, in close agreement

with thermodynamics (see Table S2 for a comparison of the dissociation temperatures for bulk and confined (from this study) methane hydrates), and v) water confined in micropores and/or narrow mesopores (R_w = 2.4) is prone to suffer a liquid-to-solid phase transition, preferentially water-to-hydrate, only in the presence of an external stimulus. In other words, high-pressure methane is able to disrupt the intermolecular bonding interactions between water molecules and/or modify the fluid - wall interactions from the Gibbs-Thomson equation, thus altering the freezing/melting performance of confined water. The similar stability of confined and bulk methane hydrates observed in the DSC scans towards dissociation is in close agreement with the phase diagram deduced experimentally for model carbon materials [27]. However, a closer look at Figure 4 and Table S2 shows that despite the similar performance, melting of confined hydrates in carbon takes place ca. 1 K below the bulk system (283 K vs. 284 K), thus suggesting that confinement effects have some influence on the water activity, i.e. confined hydrates are slightly less stable. Monte Carlo simulations of methane clathrates confined in slit-shape pores anticipated a certain instability versus bulk hydrates, in agreement with our data, although the depression in the dissociation temperature with the inverse of the pore width could not be confirmed with our data [28]. Contrarily to carbon materials, gas hydrates confined in silicas exhibit a much lower stability compared to the bulk system, the dissociation taking place at a much higher pressures or lower temperatures [29,30]. Last but not least, it is important to highlight that the results described in Figure 4 are in close agreement with the high water-to-hydrate yield described in the literature for the PPAC material and other micro/mesoporous carbon materials and the low yield obtained for bulk water under static conditions [12,30]. As a summary, Figure S5 shows a schematic drawing of the different situation taking place in each of the samples evaluated before and after incorporation of high-pressure methane.

As described above, the evaluation of the melting enthalpy can provide valuable information about the water-to-hydrate process in the presence of high-pressure methane. To this end, Table 3 compares the melting enthalpy for saturated and oversaturated PPAC samples considering exclusively the melting peak at 284 K attributed to the methane hydrate dissociation. As it can be observed in Table 3, for samples with a single contribution in the DSC profile (see samples 13 and 14 in Figure 4 lower panel), the melting enthalpy gives a value of ca. 52 kJ/mol, independently of the applied methane pressure. This enthalpy value is also preserved after a second cycle

(samples called-2). Interestingly, this value is in perfect agreement with the melting enthalpy estimated for the bulk hydrate under similar experimental conditions [31]. The excellent fitting with the theoretical value is in agreement with a complete conversion of water-to-hydrate, independently of the confinement conditions (either water confined in narrow micropores or water in wide micropores/small mesopores). This observation is really important to understand the role of the microcavities in the methane hydrate formation/dissociation process. Although nanocrystals grown in these restricted nanospaces are difficult to be identified using conventional techniques (including synchrotron XRPD), these results clearly highlight that all water confined in micropores and mesopores ($R_w \leq 4.1$) is prone to convert to gas hydrate with a high yield [12]. Contrary to silicas where a layer of liquid water is assumed to separate the solid hydrate from the pore walls, in the specific case of carbons the hydrophobic nature of the surface must promote the complete conversion due to the improved wettability of the hydrate [29]. These results confirm our previous assumptions when using activated carbon materials as a host structure and explain the superior performance of carbon materials versus other nanoporous solids such as metal-organic frameworks-MOFs, zeolites, or silicas to store methane in the form of gas hydrate [12-19,32]. Assuming -53.1 kJ/mol as the theoretical value, DSC signals can be used to estimate the phase transition yield, these values being close to 100% for those samples with water confined in micropores (saturated samples; $R_w = 2.4$) or micro/mesopores (oversaturated sample; $R_w = 4.1$). Samples with a large excess of water (sample 15; $R_w = 11$) become similar to bulk water with a small yield (below 10%).

Table 3. Enthalpy of melting calculated from the DSC experiments for the methane hydrate peak and the water-to-hydrate yield assuming the theoretical enthalpy for methane hydrate.

sample number	R_w, g_{H2O}/g_{PPAC}	Pressure, MPa	$^{*}-\Delta H_{m(hydrate)}$, kJ/mol	Water-to-hydrate conversion, %
13-1	2.4	3.5	51.9	97.7
13-2	2.4	3.5	50.0	96.0

13-1	2.4	8.0	52.5	98.9
13-2	2.4	8.0	51.5	96.9
14-1	4.1	8.0	52.0	97.9
14-2	4.1	8.0	52.4	98.6
15-1	11	8.0	4.4	8.3
15-2	11	8.0	4.4	8.4
Bulk water -1	-	3.5	4.4	2.3
Bulk water -2	-	3.5	4.5	2.4
Bulk water -1	-	8.0	7.1	3.7
Bulk water -2	-	8.0	7.8	4.1

*$\Delta H_{m(hydrate)}$ corresponds to the methane hydrate enthalpy dissociation obtained from DSC scans. Theoretical CH_4 hydrate melting enthalpy is -53.1 kJ/mol [31]

In order to get a better understanding of the anomalous freezing/melting performance in the saturated sample (R_w = 2.4), mainly the absence of water mobility to the external surface to justify the DSC contributions in the presence of high-pressure methane, the DSC experiments have been cycled under alternating high-pressure/low-pressure conditions. Figure S6 confirms the above mentioned results. Under high-pressure conditions the DSC profile shows a sharp peak at 268 K during the cooling scan, this peak shifting to higher temperature during warming (285 K). As described above, these contributions must be unambiguously attributed to methane hydrate formation and dissociation, respectively. Upon depressurization of the chamber, i.e. in the absence of methane, the DSC profile becomes completely flat. However, the freezing/melting signals are fully recovered upon a subsequent re-pressurization at 8.0 MPa. The absence of any significant shift in the freezing and melting temperatures confirm the reversibility of the process and, indirectly, the absence of water mobility under high-pressure conditions, i.e. methane hydrates nucleation and growth must take place in micropores and mesopores (including narrow micropores with sizes below the hydrate unit cell, ca. 1.21 nm). The absence of water mobility has also been evaluated using N_2 as a guest molecule under high-pressure conditions. Figure S7 show the DSC scan for the PPAC saturated sample before and after pressurization with 8.0 MPa N_2. The absence of any water-to-ice transition in both scans, cooling and heating, despite the large amount of water incorporated (2.4 g/g) clearly shows that water remains confined

in micropores, even under high pressure conditions, i.e. it remains non-freezable in the temperature range evaluated.

Last but not least, the cyclability has also been evaluated under consecutive DSC experiments, always under high-pressure conditions. Figure S8 shows that the melting of the methane hydrate is independent of the cycle, while the freezing process shifts to higher temperatures in the second cycle due to the well-known memory effect in crystallization processes. It is important to highlight that no water-to-ice transition could be observed after different cycles, i.e. the water-to-hydrate process is fully reversible and with a high yield (i.e. up to nearly 100%) after consecutive cycles [33].

3.4.2. Inelastic neutron scattering spectra (INS) of confined water under high-pressure methane

The structure of confined gas hydrates has been evaluated using inelastic neutron scattering. As described in previous papers, INS is a powerful technique for the evaluation of the confined hydrates due to the strong scattering signal of hydrogen atoms and the possibility to identify the free-rotational mode of CH_4 entrapped in small hydrate cages [12]. Figure 5 shows the INS spectra for the original PPAC carbon material, the PPAC sample after a low (R_w =0.6) and high loading of D_2O (R_w = 2.4) and the D_2O pre-adsorbed carbon after incorporation of high pressure methane (8 MPa). It was observed that the inelastic neutron scattering spectrum of the original carbon before and after adsorption of D_2O is rather flat due to the small scattering of the carbon skeleton and the deuterium atoms. However, the INS spectra change drastically after incorporation of high-pressure methane. For low- and high-D_2O loadings, i.e. for samples with D_2O pre-adsorbed in narrow micropores or samples with D_2O pre-adsorbed in micropores and small mesopores, the INS is rather similar. In both cases a strong band can be clearly appreciated at 0.99 meV, with some shoulders at 2.3 meV and 3.3 meV. These bands have already been observed for natural hydrates [34] and can be unambiguously attributed to the rotational transitions of methane from the ground state to the different excitation states [12].

In summary, INS results clearly prove the formation of methane hydrates in the confined nanospace of PPAC activated carbon, independent of the pre-adsorption ratio. The similarity between both spectra demonstrates the important role of narrow cavities (those filled at low loading) in the methane hydrate formation process. Although the

size of these cavities (below 0.7 nm) does not allow the formation of perfect crystals (taking into account that the crystal unit cell is around 1.22 nm), the presence of some defective crystals with similar characteristics to the bulk crystal could explain the obtained results [35].

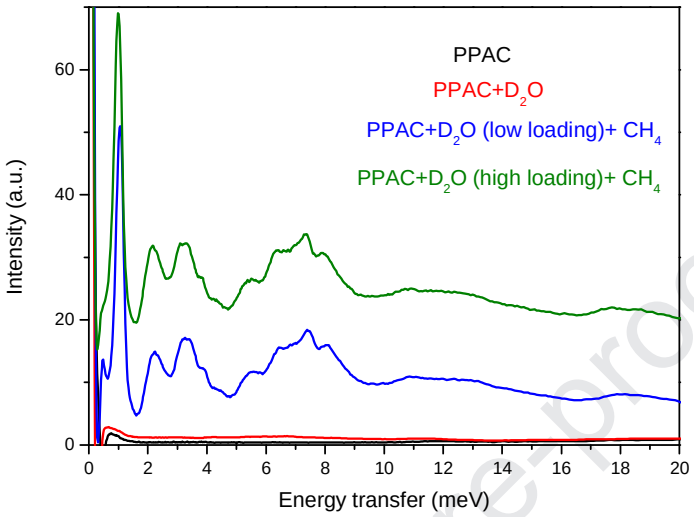

Figure 5. INS spectra of sample PPAC at 5 K before and after incorporation of D_2O, and the effect of pressurization with methane 8.0 MPa in the sample with low (R_w <0.6) and high (R_w = 4.1) D_2O loading.

3.4.3. Synchrotron X-ray powder diffraction of confined water under high-pressure methane

To end up, the crystallographic properties of the confined gas hydrates have been evaluated using in-situ synchrotron X-ray diffraction. To this end, the samples pre-adsorbed with water (R_w = 0.6 and R_w = 2.4) and evaluated in section 3.3.3, after cooling to 173 K were pressurized with 4.5 MPa of methane (maximum pressure that we can reach with the polymeric capillaries used at the synchrotron). Figure 6 show the SXRPD pattern for both sample before and after incorporation of methane.

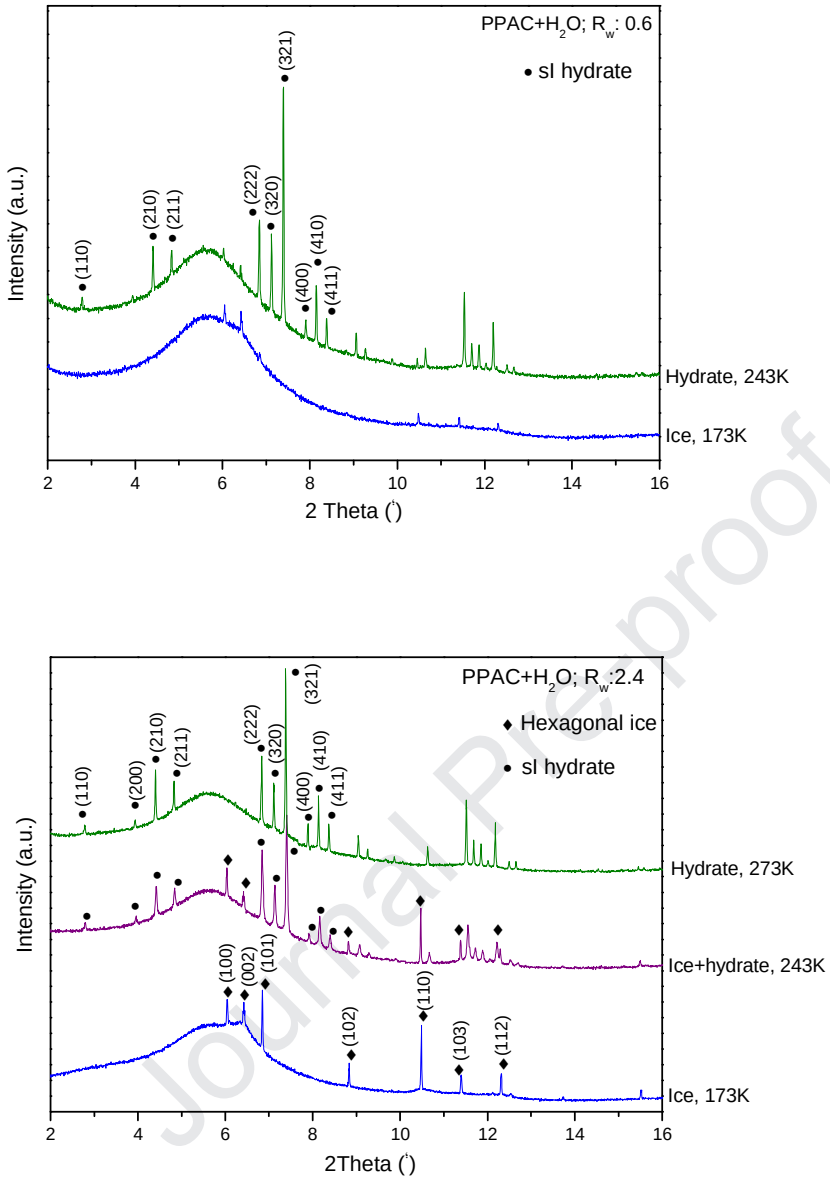

Figure 6. Synchrotron XRD profiles for the PPAC activated carbon pre-adsorbed with a low (upper panel) and high (lower panel) water content before and after incorporation of 4.5 MPa CH_4.

As described above, the XRD pattern of the undersaturated PPAC carbon (R_w = 0.6) exhibited only small peaks corresponding to distorted hexagonal ice. The absence of XRD peaks (excluding the background) was attributed to the presence of non-freezable water confined in narrow cavities. In fact, the absence of any significant signal in the DSC profile for the aforementioned sample rules out the possibility of a liquid water to

amorphous ice phase transition, as suggested in the literature for silicas with cylindrical pores [36,37]. This hypothesis is clearly demonstrated after incorporation of an external stimulus, i.e. under high-pressure methane. Although the conversion process is extremely slow at the low temperature of the measurement (173 K), a slight increase in temperature (up to 243 K under 4.5 MPa CH_4) gives rise to the sudden development of sharp peaks attributed to the sI structure of the methane hydrate. This result confirms that under these conditions (R_w = 0.6), water is indeed confined in the pores although it is non-freezable (even at 172 K), unless an external stimulus is applied, in close agreement with the DSC data. For the saturated sample the situation is rather similar. The XRD pattern of the PPAC saturated with water (R_w = 2.4) at 173 K already exhibits well-defined peaks corresponding to hexagonal ice, as described above. In this specific case, upon pressurization with methane and a slight increase in temperature, the ice peaks grow and starts to convert to sI methane hydrate, although with slower kinetics due to the experimental setup, the conversion being 100% to methane hydrate at 273 K.

4. Conclusions

Differential scanning calorimetric (DSC) measurements on a high-surface area activated carbon (PPAC) under different water-supplying conditions clearly show that the performance of confined water towards a freezing/melting phenomenon highly depends on the amount of water incorporated and the presence or not of an external stimulus. Under atmospheric pressure conditions water adsorbed in narrow cavities does not exhibit any liquid-to-solid phase transition, i.e. it is non-freezable water. On the other hand, water in larger micropores and small mesopores is prone to form ice, although at a much lower temperature compared to bulk water. This observation is in close agreement with the temperature depletion predicted by the Gibbs-Thomson equation. Under high-pressure conditions, the scenario changes drastically. In the presence of high-pressure methane the total amount of water pre-adsorbed, included water in narrow cavities, is prone to exhibit a liquid-to-solid transition, methane hydrates being formed with a yield close to 100%. The optimal performance is obtained with an adsorption ratio of R_w = 4.1, while larger values of R_w become detrimental due to the significant blocking of the pores by water and the associated slow nucleation kinetics (low water-to-hydrate yield). These results clearly explain the excellent performance of activated carbon materials

saturated or slightly oversaturated towards methane storage in the form of solid hydrates, as compared to other nanoporous systems such as zeolites and MOFs.

5. Acknowledgement

The authors would like to acknowledge financial support from the MINECO (MAT2016-80285-p), Generalitat Valenciana (PROMETEOII/2014/004), H2020 (MSCA-RISE-2016/NanoMed Project), Spanish ALBA synchrotron (Projects AV-2018022707) and Oak Ridge beam time availability (Project IPTS-20843.1).

6. References

[1]. J.H. van der Waals, J.C. Platteeuw. Clathrate solutions. Adv. Chem. Phys. 2 (1959) 1-57.

[2]. Y. Paul Handa, M. Zakrzewski, C. Fairbridge. Effect of restricted geometries on the structure and thermodynamic properties of ice. J. Phys. Chem. 96 (1992) 8594-8599.

[3]. K. Morishige, H. Yasunaga, Y. Matsutani. Effect of pore shape on freezing and melting temperatures of water. J. Phys. Chem. C 114 (2010) 4028-4035.

[4]. M. Miyahara, K.E. Gubbins. Freezing/melting phenomena for Lennard-Jones methane in slit pores: A Monte Carlo study. J. Chem. Phys. 106 (1997) 2865-2880.

[5]. A. Watanabe, T. Iiyama, K. Kaneko. Melting temperature elevation of benzene confined in graphitic micropores. Chem. Phys. Lett. 305 (1999) 71-74.

[6]. T. Iiyama, K. Nishikawa, T. Otawa, K. Kaneko. An ordered water molecular assembly structure in a slit-shaped carbon nanospace. J. Phys. Chem. 99 (1995) 10075-10076.

[7]. K. Kaneko. Molecular assembly formation in a solid nanospace. Colloids Surfaces A: Phys. Eng. Aspects 109 (1996) 319-333.

[8]. T. Iiyama, R. Aragaki, T. Urushibara, S. Ozeki. Direct determination of the intermolecular structure of the adsorbed phase using in situ X-ray diffraction and reverse Monte Carlo methods. Adsorption Science & Technology 24 (2006) 815-821.

[9]. T. Iiyama, Y. Kobayashi, K. Kaneko, S. Ozeki. In-situ small-angle X-ray scattering study of cluster formation in carbon micropores. Colloids Surfaces A: Phys. Eng. Aspects 241 (2004) 207-213.

[10]. G. Briganti, G. Rogati, A. Parmentier, M. Maccarini, F. de Luca. Neutron scattering observation of quasi-free rotations of water confined in carbon nanotubes. Scientific Reports 7 (2017) 45021.

[11]. G. Reiter, C. Burnham, D. Homouz, P.M. Platzman, J. Mayers, T. Abdul-Redah, et al. Anomalous behavior of proton zero point motion in water confined in carbon nanotubes. Phys. Rev. Letters 97 (2006) 247801.

[12]. M.E. Casco, J. Silvestre-Albero, A.J. Ramirez-Cuesta, F. Rey, J.L. Jordá, A. Bansode, et al. Methane hydrate formation in confined nanospace can surpass nature. Nature Commun. 6 (2015) 6432.

[13]. E. Andres-Garcia, A. Dikhtiarenko, F. Fauth, J. Silvestre-Albero, E.V. Ramos-Fernandez, J. Gascon, et al. Methane hydrates: Nucleation in microporous materials. Chem. Eng. J. 360 (2019) 569-576.

[14]. M.E. Casco, F. Rey, J.L. Jorda, S. Rudic, F. Fauth, M. Martinez-Escandell, et al. Paving the way for methane hydrate formation on metal-organic frameworks (MOFs). Chemical Science 7 (2016) 3658-3666.

[15]. A. Perrin, A. Celzard, J.F. Marêché, G. Furdin. Methane storage within dry and wet active carbons: A comparative study. Energy Fuels 17 (2003) 1283-1291.

[16]. L. Mu, B. Liu, H. Liu, Y. Yang, C. Sun, G. Chen. A novel method to improve the gas storage capacity of ZIF-8. J. Mater. Chem. 22 (2012) 12246-12252.

[17]. H.P. Veluswamy, A. Kumar, Y. Seo, J. Dong Lee, P. Linga. A review of solidified natural gas (SNG) technology for gas storage via clathrate hydrates. Appl. Energy 216 (2018) 262-285.

[18]. M.E. Casco, C. Cuadrado-Collados, M. Martínez-Escandell, F. Rodríguez-Reinoso, J. Silvestre-Albero, Influence of the oxygen-containing surface functional groups in the methane hydrate nucleation and growth in nanoporous carbon. Carbon 123 (2017) 299-301.

[19]. C. Cuadrado-Collados, F. Fauth, I. Such-Basañez, M. Martínez-Escandell, J. Silvestre-Albero. Methane hydrate formation in the confined nanospace of activated carbons in seawater environment. Microp. Mesop. Mater. 255 (2018) 220-225.

[20]. A.I. Kolesnikov, J.M. Zanotti, C.K. Loong, P. Thiyagarajan, A.P. Moravsky, R.O. Loutfy, et al. Anomalous soft dynamics of water in a nanotube: A revelation of nanoscale confinement. Phys. Rev. Letters 93 (2004) 035503-1

[21]. M. Sliwinska-Barthkowiak, G. Dudziak, R. Sikorski, R. Gras, K.E. Gubbins, R. Radhakrishnan. Dielectric studies of freezing behavior in porous materials: Water and methanol in activated carbon fibers. Phys. Chem. Chem. Phys. 3 (2001) 1179-1184.

[22]. M.W. Maddox, K.E. Gubbins. A molecular simulation study of freezing/melting phenomena for Lennar-Jones methane in cylindrical nanoscale pores. J. Chem. Phys. 107 (1997) 9659.

[23]. A.A. Antoniou. Phase transformations of water in porous glass. J. Phys. Chem. 68 (1964) 2754-2763.

[24]. G.G. Litvan. Phase transitions of adsorbates: 1. Specific heat and dimensional changes of the porous glass-water system. Canadian J. Chem. 44 (1996) 2617-2622.

[25]. J. Dore, M. Dunn, P. Chieux. Neutron diffraction studies of ice nucleation in porous silica. J. Phys. Colloque 48 (1987) 457-463.

[26]. K. Hofer, E. Mayer, G.P. Johari. Glass-liquid transition of water and ethylene glycol solution in poly(2-hydroxyethylmethacrylate) hydrogel. J. Phys. Chem. 94 (1990) 2689-2696.

[27]. L. Borchardt, W. Nickel, M. Casco, I. Senkovska, V. Bon, D. Wallacher, et al. Illuminating solid gas storage in confined spaces-methane hydrate formation in porous model carbons. Phys. Chem. Chem. Phys. 18 (2016) 20607-20614.

[28]. S. Nath Chakraborty, L.D. Gelb. A Monte Carlo simulation study of methane clathrate hydrates confined in slit-shaped pores. J. Phys. Chem. B 116 (2012) 2183-2197.

[29]. Y.P. Handa, D. Stupin. Thermodynamic properties and dissociation characteristics of methane and propane hydrates in 70-.ANG.-radius silica gel pores. J. Phys. Chem. 96 (1992) 8599-8603.

[30]. T. Uchida, T. Ebinuma, T. Ishizaki. Dissociation condition measurements of methane hydrate in confined small pores of porous glass. J. Phys. Chem. B 103 (1999) 3659-3662.

[31]. G.K. Anderson. Enthalpy of dissociation and hydration number of methane hydrate from the Clapeyron equation. J. Chem. Thermodynamics 36 (2004) 1119-1127.

[32]. L. Borchardt, M.E. Casco, J. Silvestre-Albero. Methane hydrate in confined spaces: An alternative storage system. ChemPhysChem 19 (2018) 1298-1314.

[33]. M.E. Casco, J.L. Jordá, F. Rey, F. Fauth, M. Martinez-Escandell, F. Rodriguez-Reinoso, et al. High-performance of gas hydrates in confined nanospace for reversible CH_4/CO_2 storage. Chemistry: A European J. 22 (2016) 10028-10035.

[34]. C. Gutt, B. Asmussen, W. Press, C. Merkl, H. Casalta, J. Greinert, et al. Quantum rotations in natural methane-clathrates from the Pacific sea-flor. Europhys. Lett. 48 (1999) 269-275.

[35]. J. Miyawaki, T. Kanda, T. Suzuki, T. Okui, Y. Maeda, K. Kaneko. Macroscopic evidence of enhanced formation of methane nanohydrates in hydrophobic nanospaces. J. Phys. Chem. B 102 (1998) 2187-2192.

[36]. D. Morineau, G. Dosseh, C. Alba-Simionesco, P. Llewellyn. Glass transition, freezing and melting of liquids confined in the mesoporous silicate MCM-41. Philos. Mag. B 79 (1999) 1847-1855.

[37]. R. Radhakrishnan, K.E. Gubbins, M. Sliwinska-Bartkoviak. Global phase diagrams for freezing in porous media. J. Chem. Phys. 116 (2002) 1147-1155.

Universidad de Alicante
Departamento de Química Inorgánica

Laboratorio de Materiales Avanzados

Dr. Joaquín Silvestre Albero

Alicante, 23rd September 2019

Editor
CARBON

Declaration of Interest Statement

Dear Editor,

We confirm that our manuscript entitled "Freezing/melting of water in the confined nanospace of carbon materials: Effect of an external stimulus" by C. Cuadrado-Collados, A.A. Majid, M. Martinez-Escandell, L.L. Daemen, A. Missyul, C. Koh and J. Silvestre-Albero has not been published before in any other journal, that it is not under consideration for publication elsewhere, that its publication is approved by all authors and tacitly or explicitly by the responsible authorities where the work was carried out, and that, if accepted, it will not be published elsewhere in the same form, in English or in any other language, including electronically without the written consent of the copyright-holder.

With best regards,

Prof. Joaquín Silvestre-Albero
University of Alicante (Spain)

Campus San Vicente del Raspeig. Apartado 99. E-03080 Alicante. Spain
Phone: 34 96 5909350. Fax: 34 96 5903454. E-Mail: joaquin.silvestre@ua.es